The time and temperature dependences of the stress recovery of Ecoflex polymer

Zisheng Liao, Jie Yang, Mokarram Hossain, Grégory Chagnon, Xiaohu Yao

The time and temperature dependences of the stress recovery of Ecoflex polymer

Zisheng Liao [a,b,1], Jie Yang [a,b,1], Mokarram Hossain [b,*], Gregory Chagnon [c], Xiaohu Yao [a,*]

[a] *State Key Laboratory of Subtropical Building Science, South China University of Technology, Guangzhou 510640, China*
[b] *Zienkiewicz Centre for Computational Engineering, College of Engineering, Swansea University, SA1 8EN, United Kingdom*
[c] *University of Grenoble Alpes, CNRS, UMR 5525, VetAgro Sup, Grenoble INP, TIMC, 38000 Grenoble, France*

ARTICLE INFO

ABSTRACT

Ecoflex silicone rubbers, served as the polymeric components of flexible electronic devices, actuators, energy converters, etc., are subjected to repetitive loadings during their service lives. The resulting stress softening and stress recovery phenomena can impose complicated impacts on their actual performances. Therefore, the importance of a better understanding of these phenomena needs to be stressed. In this contribution, we focus on the stress recovery behaviour of the Ecoflex silicone rubber in consideration of time and temperature dependences. Our findings show the time–temperature equivalence of the stress recovery behaviour. Based on the experimental study, a constitutive model is developed at finite strains using the Time–Temperature Superposition (TTS) principle to capture both the time and temperature dependences of the stress recovery behaviour of Ecoflex.

1. Introduction

Silicone polymers have intense applications in biomechanical science thanks to their bio-medical friendly properties such as non-toxicity, non-reactiveness, and bio-compatibility [1]. These properties reduce the risk of human tissue rejection and inflammation, making silicone ideal for the use in mechanobiological equipment [2]. Furthermore, the high stretchability and durability of silicone polymers provide a mechanical compliance matching biological tissues such as human skin [3,4], which facilitates their employment in fields including cushioning, prosthetics [5], synthetic vascular grafts [6], and soft sensors [7–9]. Among different silicone rubbers, the commercially available dielectric silicone rubber Ecoflex™ series (Smooth-On, USA) has been frequently used in wearable flexible strain sensor for epidermal electrical systems [6,10–14]. Other applications include soft robotics [15–18], insulations for electric power devices [6,19], flexible energy harvester [20–22], etc.

During the operation of these applications, repetitive loadings on the silicone components cause stress softening, i.e., the Mullins effect, and afterwards, stress recovery behaviour. Such effects introduce changes in mechanical behaviour that can affect material performances during their service lives, which necessitates a comprehensive understanding of stress softening and stress recovery phenomena. Mullins [23] discovered that when filled rubbers are re-stretched to

the same maximum strain, the overall stress level drops significantly lower than the pre-stretched path, while the peak stress points of both stretches are close to each other. This behaviour, which is known as stress softening or the Mullins effect, has been extensively studied through experiments [17,24–27] and constitutive modellings [28–35]. In our previous studies [36,37], we also clearly observed and subsequently characterised the stress softening behaviour in the Ecoflex polymer series.

It is worth noting that the stress softening is completely or partially reversible for many filler polymers. This phenomenon is called stress recovery. As discovered by Mullins [23], after annealing the stretched or softened filled rubber samples at various annealing temperatures and times, the stress levels recovered to varying extents, and stress softening can be observed again in the subsequent stretch cycles. This suggests that stress recovery is a time- and temperature-dependent process. Rigbi [38] reported a partial recovery in the reloading process of carbon-black-filled rubbers at room temperature four weeks following the first cycle. Yan et al. [39] observed a complete stress recovery of the nanoparticle-filled PDMS polymer that was subjected to a simple shear loading. The recovery has also been observed by Zheng et al. [40] in the tough gels at a faster rate than in filled rubbers. Our previous study [41] also observed the stress recovery behaviour at ambient temperature with a variety of Shore hardnesses and deformation modes. Mullins found that the stress recovery is

---

slow at the ambient temperature, while it is accelerated significantly at elevated annealing temperatures [23]. According to Laraba-Abbes et al. [42], carbon-black filled natural rubbers underwent a complete recovery after a 95 °C annealing for two days. As reported by Diani et al. [43], carbon-black filled styrene-butadiene-rubbers (SBR) also recovered completely after 17-hour annealing at 80 °C. Amin et al. [44] found that there is a threshold temperature for the full recovery of filler-reinforced natural rubber/polybutadiene rubber blends. Plagge and Klüppel [45] discovered temperature-induced stress recovery in a strain-crystallising natural rubber (NR) and various non-crystallising rubbers (such as ethylene-propylene-diene (EPDM), hydrated-nitrile-butadiene rubber (HNBR), and SBR) with various filler concentrations of carbon black or silica. Harwood and Payne [24] discovered that swelling natural rubber in solvents also enables its stress recovery.

Extensive research on stress softening and stress recovery in the literature draws various conclusions about the microscopic mechanisms of these two successive behaviours. There are some common points of views [1,43,46–48]:

1. chain scission, cross-link or physical bond breakage,
2. disentanglement,
3. agglomerate fracture of the filler domain,
4. filler-rubber dissociating and re-associating interactions, and
5. the combination of above.

For example, some studies adopted the limiting chain extensibility theory, i.e., bonds breaking [49–53] while Mullins' [23] work showed a different scenarios. According to his investigation, the existence of fillers was found to increase the stiffness, electric conductivity, and power factor. These properties were observed to decrease after the specimen was flexed or stretched and tended to recover to the initial state at a faster rate at a higher temperature. Accordingly, it is concluded that the breakdown of agglomerates and chains of filler particles is responsible for the stress softening, while the stress recovery is attributed to the re-adsorption of the filler particles. Other studies also found correlations between the filler-matrix interactions and the stress softening and stress recovery behaviours. For instance, Blanchard and Parkinson [54] suggested that the shear modulus degradation is due to the crosslinks decreasing when filler-rubber linkages break. Drozdov and Dorfmann [55] also correlated stress softening with crystallisation in the filler-rubber interaction region. Yan et al. [39] suggested that the re-establishment of the filler-network structures, such as filler-chain reconnection and the formation of new entanglements, contributes to stress recovery. These filler-rubber dissociating and re-associating interactions of filler reinforced polymers are the main sources of the stress softening and the stress recovery, respectively. This has been supported by swelling tests [48,56], where the results showed that no significant cross-link or chain breaks after stretching. The diversified explanation shows that the actual micro-mechanism of the Mullins effect is complex and remains controversial since in situ observation of the microstructure evolution is technically difficult at present.

Regardless of extensive experimental research on the stress softening and stress recovery behaviours, only a few studies develop constitutive models to characterise stress recovery after stress softening. Drozdov and Dorfmann [55] developed a constitutive model combining a permanent network and a temporary network in a composite manner. They characterised the stress softening and stress recovery behaviours by depicting the temporary networks with a rate of breakage function and a rate of reformation function of junctions, both of which are dependent on time and the energy of breakage. The calibration of the experimental data was carried out separately on pre-stretch and re-stretches. De Tommasi et al. [50–53,57] developed micromechanical models to describe stress softening and stress recovery behaviours of rubbery materials. They assumed that a polymer system is composed of a series of elastic chains as well as breakable chains. The breakable chains activate and fracture (or transform phase) at certain total strain levels following certain distributions. The stresses of all the activated chains contribute to the total stress response. In their framework, the breakage or transformation of chains causes stress softening. They further assume that when the polymer is unloaded to a strain value lower than the activation threshold strain, the chains broken previously would rebond immediately at a given ratio, leading to stress recovery. Long et al. [58] also obtain the total stress response by summing up the stresses of activated chains. They gave different assumptions that all virgin chains activate at the beginning of loading, and debond from the polymer network at a rate related to the concentration of activated chains regardless of applied strain level, which causes stress softening. The debonded chains are assumed to relax immediately to an unstretched state, and then rebond to the network at a rate that depends on the concentration of debonded chains. The rebonded chains will be reactivated when loading continues. Therefore, debonding and rebonding, or stress softening and stress recovery happen during the whole course of loading and unloading. Wang and Chester [59] developed a thermo-mechanically coupled constitutive model incorporating the idea of a hard-to-soft phase transition. The deformation of soft domains is considered as an amplification of the hard domain of an equivalent mass, according to [60]. The hard domains convert to soft domains during stress softening, while the reversed process happens during thermal stress recovery. These two competing processes contribute to the evolution of the volume fraction of soft domains. Chu et al. [61] proposed a micromechanical model concerning the evolution of the filled polymer networks to describe stress softening and its recovery. They adopted a temperature-dependent network density coefficient of the strain energy function according to [62], which also undergoes competing evolution due to the dynamical damage and repair of the polymer network. Lamont et al. [63] proposed a statistical model based on their previous work [64], which evaluates the distributions of chains in attached, detached, and ruptured states. Stress softening and stress recovery are characterised by the evolutions of statistical concentrations of the effective chains due to chain detachment and re-attachment. Note that many polymers exhibit time–temperature equivalence in many mechanical properties, such as their storage and loss modulus [65]. The roles of increasing the annealing temperature and accelerating the recovery have not been considered in the view of time–temperature equivalence. In addition, the relationship between the annealing time and annealing temperature has not been quantified and modelled yet.

Since stress softening and stress recovery influence the performance of the material appliance, a comprehensive investigation of the mechanical behaviour and constitutive modelling of stress softening and stress recovery is necessary. In this manuscript, to investigate the time and temperature dependences of stress softening and stress recovery phenomena, annealing is applied to the specimens at various temperatures with various periods between the two cycles of loading–unloading experiments. The constitutive relationship, in conjunction with the time and temperature dependences, is developed using Time–Temperature Superposition (TTS) principle and calibrated according to the experimental results. Section 2 presents the experimental details and the schedule. Section 3 illustrates the experimental results, gives an analysis of the time dependence and the temperature dependence of stress recovery, and evaluates their equivalence. Section 4 introduces a TTS model to capture the stress recovery behaviour. Finally, in Section 5, we provide an overview of this work.

2. Experimental preliminaries

The platinum-catalysed Ecoflex^{TM} (Smooth-on, USA) is a group of commercially available silicone rubbers with several available hardnesses (e.g., 00–50, 00–30, 00–20, 00–10) with different ratios of fillers. They are two-component silicones, curing at ambient temperature with negligible shrinkage and in a relatively short time, from several minutes to several hours. According to [17], the Ecoflex silicone rubbers of hardness Shore 00-30 are investigated in this contribution. Ecoflex 00-30 has a filler ratio of about 30% and a gel fraction of 44% wt/wt. By
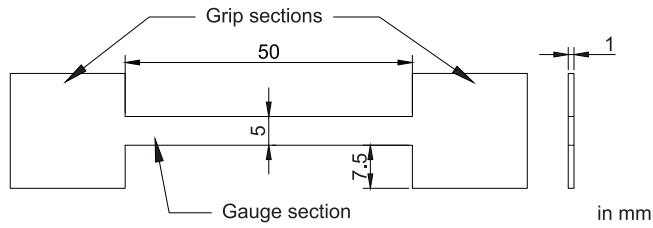
Fig. 1. The shape and dimension of the uniaxial tension specimen. A 50 mm × 5 mm × 1 mm (length × width × thickness) gauge section is adopted.

Fig. 2. Schematic of the definition of energy density [41]. (For interpretation of the references to colour in this figure legend, the reader is referred to the web version of this article.)

mixing the liquid premixes of part A and part B in a 1:1 volumetric ratio, the reaction of polymer, crosslinker, and platinum catalyst is enabled. After curing for over 24 h in a designed specimen mould, the specimens are ready for experiments.

Rectangular specimens with a 50 mm × 5 mm × 1 mm (length × width × thickness) gauge section are utilised as specified in Fig. 1. This geometry is the same as the uniaxial tension specimen used in our previous work [41], under which the deformation is considered uniform. Rectangular specimens are also used in the literature, see [66–68]. The specimens are glued to aluminium shims to ensure a tight grasp and avoid the deformation of the clamping parts. We use a rectangular shape to minimise the error introduced by the fillet section of a dumbbell specimen since we do not consider specimen failures. It should be noted that the localisation effect, a typical characteristic for filled polymers [69–71], is not included in our contribution. This effect occurs when the material undergoes strain softening during loading, especially for glassy polymer [72,73]. Nevertheless, the material investigated in this contribution is a rubbery material, and the stress increases monotonically during stretching. Therefore, the deformation is generally uniform and no obvious localisation effect is observed, similar to other soft polymers [67,74].

Cyclic loadings are exerted on the specimens by an Instron 5567 universal test machine with a ± 50 N force sensor. For the annealing process, a temperature chamber is employed to regulate the annealing temperature and annealing time.

Our previous work about the stress recovery of the Ecoflex polymer [41] employed two-cycle loading–unloading tests and compared the stress levels as well as the energy dissipation densities of stress softening between the two cycles. Following this approach, in the current study, we further investigate the time and temperature influences on the stress recovery by annealing the specimens between the two cycles of loading–unloading at varying temperatures (i.e., 0 °C, 20 °C, 40 °C, and 60 °C) and times (i.e., 0 h, 1 h, 24 h, and 168 h), as arranged in Table 1. Specifically, a primary loading–unloading tension (named "pre-stretch") is applied to a virgin sample at room temperature. This is followed by the annealing process in a separate temperature chamber at a specified temperature for a specified time (see Table 1), where stress recovery occurs. Afterwards, the sample is remounted to the test machine and a secondary loading–unloading (named "re-stretch") tension is applied. Through this procedure, the influence of the annealing process on the level of stress recovery is investigated.

Both pre-stretch and re-stretch are loaded under the uniaxial tension mode at 20 °C and a fixed strain rate of 0.1 /s. In addition, each specimen is stretched up to a common strain level of 400%. Note that in our previous study [36], time dependence of the stress softening was observed, where a lower strain rate leads to a longer softening time and therefore a stronger stress decrease. In addition, stronger stress softening was also observed in the condition of a larger maximum strain level. Both the strain rate and the maximum strain level determine the extent of the stress softening. In this manuscript, since our focus is on the time and temperature dependence of the stress recovery instead of the stress softening, a single pair of strain rate and maximum extension corresponding to a certain softening level is chosen. The experiment
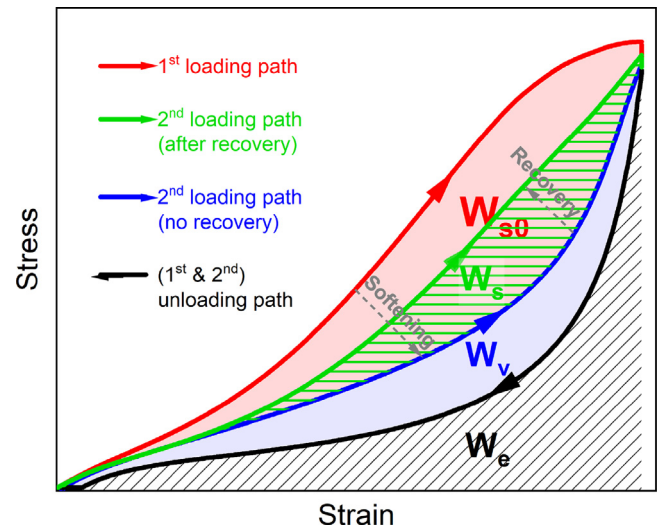
is repeated at least five times to ensure reproducibility. Error bars are used to present the data fluctuation in the experimental results. Our experiment data is recorded using nominal stresses (known as the first Piola–Kirchhoff stresses) and nominal strains (known as the engineering strains). Note that the nominal strain is measured as the crosshead displacement divided by the initial length (50 mm) of the specimen.

3. Results and discussion

3.1. Definitions and notes

The experiments carried out in this contribution are mainly loading–unloading cyclic tests. As the schematic Fig. 2 illustrates, the loading–unloading path of a cycle forms a loop, and its area quantifies the energy dissipation density, i.e.,

$$w = \int_l \sigma d\varepsilon, \qquad (1)$$

where l is the loading–unloading path of a cycle, and σ and ε are the nominal stress and nominal strain, respectively. Li et al. [48] reported that the total energy dissipation of a filled rubber material is decomposed into two parts: a recovery hysteresis part and a softening part. Our previous contribution [41] also discovered that the dissipation during cyclic tensile deformation of Ecoflex consists of a viscoelastic (i.e., recovery hysteresis) part and a softening part related to stress softening and recovery.

As Fig. 2 shows, the red loading path and the black unloading path comprise the pre-stretch (the first cycle) applied to a virgin specimen. When a re-stretch (second cycle) is applied immediately after the pre-stretch, the stress level of the loading path (the path in blue) drops, while the unloading path almost overlaps with that of the pre-stretch. Here, the second loading path divides the area of the pre-stretch cycle into a red area and a blue area. The red area w_{s_0} disappears in the immediately applied re-stretch, indicating that stress softening occurs in the pre-stretch process, and this area is considered the initial softening dissipation density part. The remaining blue area w_v is contributed mainly by the viscoelasticity, which is the energy dissipation density of the immediately applied re-stretch. Therefore, the initial softening dissipation can be denoted by

$$w_{s_0} = \int_{l_0} \sigma d\varepsilon - \int_{l_{lim}} \sigma d\varepsilon, \qquad (2)$$

Table 1

The schedule of the annealing experiments on the Ecoflex silicone rubbers.

Deformation mode	Strain rate	Strain level	Shore hardness	Annealing time	Annealing temperature			
					0 °C	20 °C	40 °C	60 °C
Uniaxial tension	0.1 /s	400%	00–30	0 h	•	•	•	•
				1 h	•	•	•	•
				24 h (1 day)	•	•	•	•
				168 h (1 week)	•	•	•	•

where l_0 is the loading–unloading path of the pre-stretch, and l_{im} is the loading–unloading path of the immediately applied re-stretch. As explained in our previous work [41], we suppose that at the immediately applied re-stretch, the dissipation is mainly caused by viscoelasticity as minimum stress recovery takes place.

If stress-free annealing is applied to a pre-stretched specimen, stress recovery occurs. On the loading path of a re-stretch after annealing (the path in green), the stress level recovers towards the loading path of the pre-stretch (the path in red), which indicates that stress softening is recoverable. The blue path divides this re-stretch cycle into two regions again. The green area w_s is the partially reversed stress softening part, causing softening dissipation again during this re-stretch. If an immediate cycle is applied to this re-stretched specimen again, it disappears again, and only the blue area remains. This subsequent softening dissipation can be denoted by

$$w_s = \int_l \sigma d\varepsilon - \int_{l_{im}} \sigma d\varepsilon, \tag{3}$$

where l is the loading–unloading path of the re-stretch after annealing for a specified duration at a specified temperature. According to this definition, for the immediately applied re-stretch, $w_s = 0$.

Note that the total response can be interpreted by polymer physics. The area below the unloading path, w_e, is the hyperelastic energy that can be fully recovered after unloading. This part corresponds to the entropic change of the backbone of the polymer network [75]. The viscoelasticity part, w_v, is thought to be created by the dangling chains and the sol fraction of an off-stoichiometric imperfect polymer network [1,48]. These chains slip and cause internal friction and energy dissipation during deformation. In terms of the part that undergoes stress softening and recovery, w_s, is thought to be contributed by filler-matrix bonds (or other physical and chemical bonds) breakage and reconnection, which has been mentioned previously in Section 1.

As mentioned above, during each cycle of the stretch (pre-stretch or re-stretch), the dissipation density can be decoupled into two parts, i.e., stress softening part (w_{s_0} or w_s) and viscoelasticity (w_v). These two parts are quantitatively regionalised as Fig. 2 shows. Here, the viscoelastic dissipation is characterised by the immediate re-stretch cycle. Note that the stress does not fully soften in the pre-stretch cycle [58,76]. Nevertheless, it is observed that stress decreases within subsequent cycles are not significant compared to the pre-stretch cycle [41,46]. Furthermore, stress also decreases due to the existence of viscoelasticity, which means applying more cycles does not help much with decoupling these two parts. For simplicity, only one-cycle pre-stretch and one-cycle re-stretch is applied.

3.2. Stress recovery with various annealing times and temperatures

First, tests at a common annealing temperature of 60 °C are applied to the pre-stretched specimens to demonstrate the stress recovery with time. Both pre-stretch and re-stretch are at the same strain rate of 0.1 /s and the same strain level of 400%. In our previous findings [41], at ambient temperature, the loading path of the re-stretch curve approaches that of the pre-stretch curve upon the increase in annealing time, indicating that the decreased stress and the energy dissipation due to the stress softening can recover with time. In this work, we have similar findings at different annealing temperatures. Fig. 3 depicts the stress recovery of the stress level in terms of the stress–strain curve at
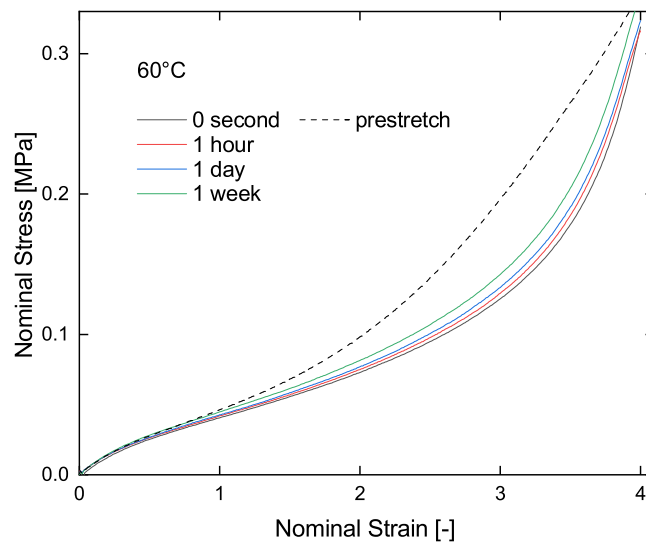

Fig. 3. Annealing at 60 °C with different annealing times. The dashed curve is the representative pre-stretch and the solid curves are the re-stretches after annealing.

an annealing temperature of 60 °C. Note that the unloading paths are almost overlapped, which is consistent to our previous studies [36,37, 41]. This means that the unloading is rate-independent, both before and after the recovery. Since the unloading path are almost overlapped, for a clear presentation, only the loading paths of the pre-stretch and the re-stretch cycles are plotted. This means that the stress recovery process is accumulated when the specimen is annealed for a longer duration, which indicates the annealing time dependence of the stress recovery.

Tests with a common annealing time of 1 week are then applied to the pre-stretched specimens to demonstrate the temperature influence of the stress recovery. The recovery speed varies to annealing temperatures. Higher recovery extents can be seen in re-stretches at higher annealing temperatures. Fig. 4 depicts the stress recovery of the stress level in terms of the stress–strain curve at an annealing time of 1 week. Only the loading paths of the pre-stretch and the re-stretch cycles are plotted for the same reason as Fig. 3. The results show that the stress recovery process is promoted when the specimen is annealed at an elevated temperature, which indicates the annealing temperature dependence of the stress recovery.

The comparison of the stress–strain curves of the loading path gives us an intuitive understanding of the time (as Fig. 3 shows) and temperature (as Fig. 4 shows) dependences of the stress recovery behaviour. That means, at a larger annealing time and a higher annealing temperature, the recovery effect is more distinct.

To identify the degree of stress recovery, the ratio of softening dissipation density between the re-stretch cycle after annealing w_s and the pre-stretch cycle on the virgin specimen w_{s_0}, is calculated as w_s/w_{s_0}. The temperature dependence of the recovery can be identified in Fig. 5. At a higher temperature, the increase in dissipation of softening w_s (the left vertical axis) and therefore the degree of recovery w_s/w_{s_0} (the right vertical axis) can be observed concerning each annealing time. Moreover, the distance between different annealing times expands upon the increase in annealing temperature, which indicates the acceleration of recovery.
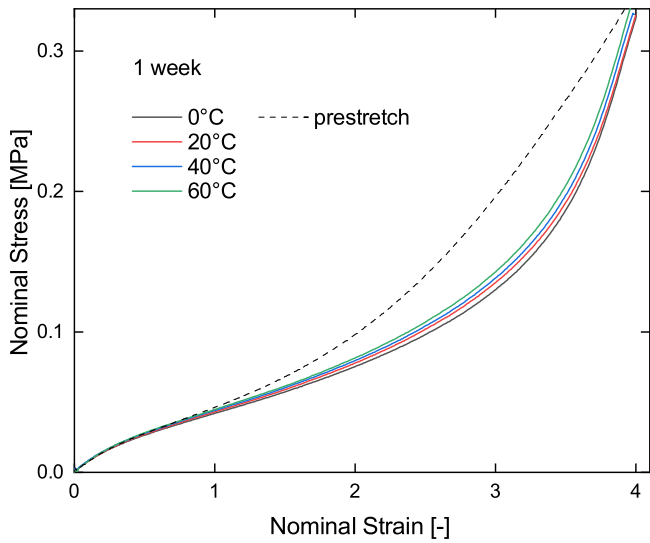
Fig. 4. Annealing for 1 week at different annealing temperatures. The dashed curve is the representative pre-stretch and the solid curves are the re-stretches after annealing.
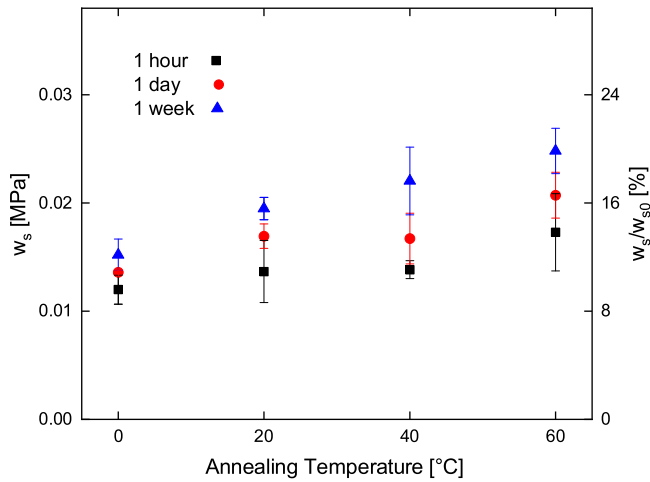

Fig. 5. Dissipation densities versus annealing temperatures. Different annealing times are highlighted by shapes and colours of symbols.
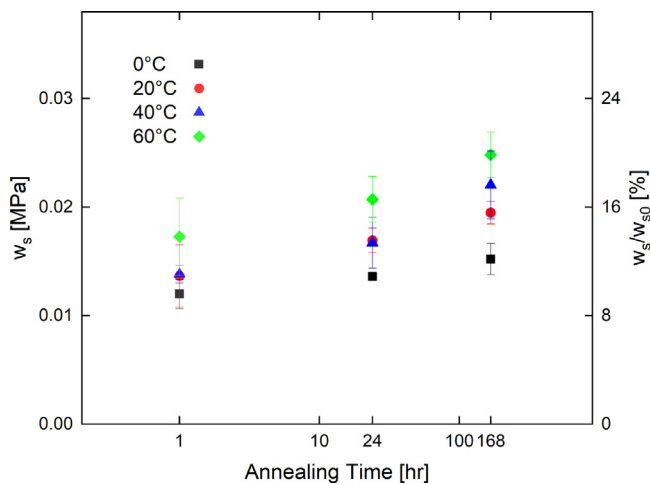

Fig. 6. Dissipation densities versus annealing time. Different annealing temperatures are highlighted by shapes and colours of symbols.
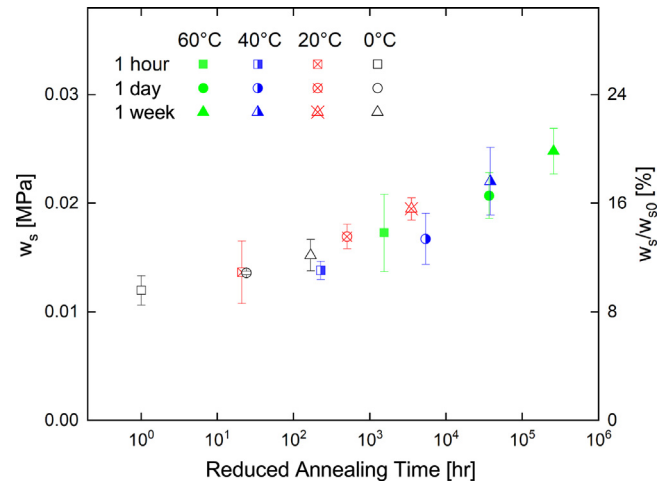

Fig. 7. Dissipation densities versus reduced annealing time using TTS principle.

Similarly, the time dependence of recovery can also be identified, as is shown in Fig. 6. Note that Fig. 6 is plotted under the logarithmic horizontal axis. The recovery accumulates with time, leading to an increase in the dissipation of the softening part in the subsequent cycles. Moreover, the rate of recovery is faster at higher annealing temperatures, and therefore the data points expand, which also indicates the acceleration of recovery.

3.3. Time–temperature equivalence of the stress recovery behaviour

As the description in Section 3.2 shows, the recovery behaviour shares a similar dependence on time and temperature, which reminds us of the classical TTS principle of the behaviour of polymeric materials. According to polymer physics, the property of thermal motion of molecular renders the same relaxation phenomena taking place either for a longer time at a lower temperature or for a shorter time at a higher temperature [77]. The viscoelasticity behaviour, including creep, stress relaxation, and dynamic mechanical analysis, follows the TTS principle [78]. Our experimental results suggest that stress recovery also follows this principle. Based on the TTS principle, the variation of temperature can be regarded as a shift of time in the logarithmic horizontal axis. If we define the new horizontal axis as the reduced annealing time t_r after using the TTS principle, it can be expressed as

$$t_r = t/a_T, \qquad (4)$$

or

$$\log(t_r) = \log(t) - \log(a_T), \qquad (5)$$

where the shift factor a_T, which determines the amount of shift at different temperatures, can be obtained by the Williams–Landel–Ferry (WLF) equation [77,79]

$$\log(a_T) = -\frac{C_1 \left[T - T_{\text{ref}} \right]}{C_2 + T - T_{\text{ref}}}, \qquad (6)$$

where T_{ref} is the reference temperature, and C_1, C_2 are material parameters. We use $T_{\text{ref}} = 0°\text{C} = 273.15$ K in this contribution. By using the method in line with [65,74], $C_1 = 24.9$ K and $C_2 = 143.7$ K are obtained. Fig. 7 shows the data points after applying the TTS principle under the reduced annealing time axis. All points basically fall into a single line, which means the time and temperature have an equivalent effect on the recovery behaviour.

Similar to the explanation in [46,80], we also suggest that the external stress lowers the energy barriers for the breakage of filler-rubber bonds. As a result, providing a greater possibility of bonds to surpass the barriers, leading to bond breakage and stress softening at

a certain rate. The breakage accumulates as time increases. Upon the reduction or removal of the external stress, the energy barriers reverse and the rate of bond rebuilding becomes dominant, following a certain evolution pattern [52,53,58,63]. As a result, stress recovery takes place. Similarly, the rebonding also accumulates as time evolves. The stress softening and the stress recovery compete during the whole course of loading and unloading [58]. As seen from the experimental results, the extent of the stress recovery can be increased when annealing the system to a higher temperature for a longer time. This is because that the elevated temperature promotes the thermal molecular motion, which increases the mobility of reaching the stable rebonding state, while the annealing time allows sufficient possibility (or concentration) of rebonding. This microscopic process corresponds to the acceleration of the evolution rate of the stress recovery at the macroscopic level at higher annealing temperatures and longer annealing time, as can be seen in our experiment. The correlation between stress recovery and thermal molecular motion legitimises the time–temperature equivalence behaviour of the stress recovery phenomenon.

4. A constitutive model of stress recovery based on the TTS principle

With the discovery of the time–temperature equivalence of the stress recovery behaviour in Section 3.3, a simple but robust model of stress recovery can be developed on the basis of the stress softening model in our previous work [37]. To begin with, the partial derivative of the coordination of the current configuration x with respect to the coordination of the original configuration X, i.e., the deformation gradient $\mathbf{F} = \frac{\partial x}{\partial X}$ is introduced. The left Cauchy–Green strain tensor, defined as $\mathbf{b} = \mathbf{F}\mathbf{F}^T$, is used to characterise the large deformation of materials. Note that many rubbery materials, including Ecoflex silicone rubbers, are conventionally considered incompressible. In this case, the third invariant of $\mathbf{b}$ becomes unity, i.e., $I_3 = 1$. The response of polymeric materials can be characterised by a strain energy function that is dependent on the invariants of $\mathbf{b}$. As $I_3 = 1$, the strain energy function is only dependent on I_1 and I_2. To further simplify the model, the first-invariant based energy function $\Psi = \tilde{\Psi}(I_1)$ is considered. Two widely-used classical energy functions, i.e., Neo-Hooke (NH) and Yeoh (Y) models, are used here. The Neo-Hooke and Yeoh energy functions are

$$\Psi_{\mathrm{NH}} = \frac{\mu}{2}\left[I_1 - 3\right],\tag{7}$$

$$\Psi_{\mathrm{Y}} = c_1\left[I_1 - 3\right] + c_2\left[I_1 - 3\right]^2 + c_3\left[I_1 - 3\right]^3,\tag{8}$$

where μ, c_1, c_2, c_3 are material parameters. When Ψ is only dependent on I_1, the Cauchy stress can be expressed as

$$\boldsymbol{\sigma} = -p\mathbf{I} + 2\frac{\partial\Psi}{\partial I_1}\mathbf{b},\tag{9}$$

where p is a scalar Lagrange multiplier, which will be determined by appropriate boundary conditions [81,82]. Note that under the uniaxial deformation mode, $I_1 = 2\lambda^{-1} + \lambda^2$, where λ is the elongation in the uniaxial direction. Applying Eq. (9), the Cauchy stress expressions of the two models under uniaxial tension mode can be derived as

$$\sigma_{\mathrm{NH}} = \mu\left[\lambda^2 - \lambda^{-1}\right],\tag{10}$$

$$\sigma_{\mathrm{Y}} = \left[2c_1 + 4c_2\left[I_1 - 3\right] + 6c_3\left[I_1 - 3\right]^2\right]\left[\lambda^2 - \lambda^{-1}\right].\tag{11}$$

The first Piola stress tensor (nominal stress tensor) is related to the Cauchy stress tensor by

$$\mathbf{P} = \det\mathbf{F}\left[\mathbf{F}^{-1}\boldsymbol{\sigma}\right],\tag{12}$$

and under a uniaxial deformation for incompressible materials, this relation is given by $P = \lambda^{-1}\sigma$. Then we have

$$P_{\mathrm{NH}} = \mu\left[\lambda - \lambda^{-2}\right],\tag{13}$$

$$P_{\mathrm{Y}} = \left[2c_1 + 4c_2\left[I_1 - 3\right] + 6c_3\left[I_1 - 3\right]^2\right]\left[\lambda - \lambda^{-2}\right].\tag{14}$$
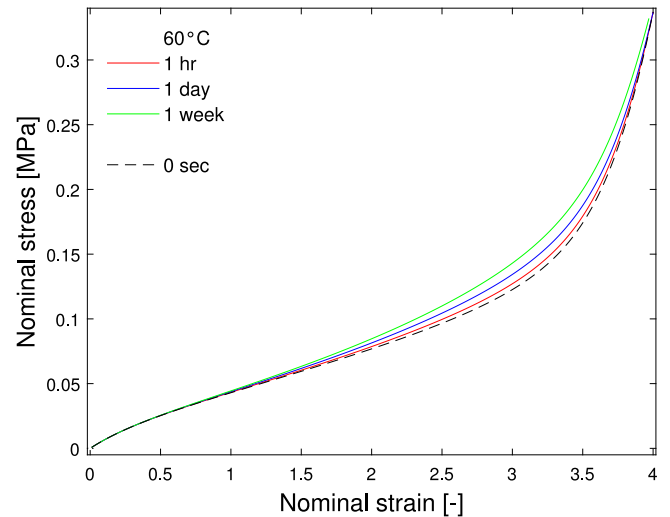

Fig. 8. Modelling results of the stress–strain curves of re-stretches after different annealing times.

Here, we consider that the mechanical response is composed of a equilibrium part and a overstress part, which are time-independent and time-dependent, respectively. The stress softening only takes place in the overstress part. A coefficient function η is introduced to represent the stress softening based on Ogden and Roxburgh's work [28]. The model under uniaxial tension state is written as:

$$P = P^{\mathrm{NH}} + \eta P^{\mathrm{Y}} = \mu\left[\lambda - \lambda^{-2}\right] + \eta\left[2c_1 + 4c_2\left[I_1 - 3\right]\right.$$
$$\left. + 6c_3\left[I_1 - 3\right]^2\right]\left[\lambda - \lambda^{-2}\right],\tag{15a}$$

$$\eta = 1 - \frac{1}{r}\tanh\left(\frac{\Psi_{\mathrm{Y}}(I_{1,\max}) - \Psi_{\mathrm{Y}}(I_1)}{\mu_0 m}\right),\tag{15b}$$

where $I_{1,\max}$ is the historical maximum value of the first strain invariant, r, μ_0 and m are material parameters. The Neo-Hooke model serves as an equilibrium part, while the Yeoh model represents the virgin state of the overstress part in Eq. (15a). Note that the amplification factor for the Shore variation [37] is normalised and is not presented here since we investigate only one Shore hardness 00-30.

$\eta \leq 1$ in Eq. (15b) is the internal variable that determines the stress level compared to the original state after the stress softening. When $I_{1,\max}$ evolves, the stress softening effect is intensified at an I_1 that is smaller than $I_{1,\max}$. As we found in our experiments, the stress of specimens is gradually recovered during annealing, which means that the stress softening is reversing. Therefore, one can consider that the total level of η approaches 1 as recovery happens. To this end, we adjust the parameter r to a concise and effective expression:

$$r = r_0\left[1 + \alpha\left[\frac{t_{\mathrm{r}}}{t_0}\right]^n\right],\tag{16}$$

where α and n are two more dimensionless parameters that are to be determined using experimental data. At the beginning of the annealing, $t_{\mathrm{r}} = 0$ and therefore $r = r_0$, meaning that stress softening just happens. As time evolves, η approaches zero when t_{r} approaches infinity, which represents a tendency for complete recovery after an infinity annealing time. Note that the variable t_{r} is the reduced annealing time, as we apply the TTS principle Eqs. (4) and (6) here. In this case, when temperature increases, t_{r} also increases, showing an equivalent effect of a time increase.

Fitting Eq. (15) using experimental results in Fig. 3 at different annealing times, the values of the parameters $\alpha = 2.818 \times 10^{-2}$ and $n = 1.991 \times 10^{-1}$ are obtained. The stress recovery is nicely predicted by the simulation curves shown in Fig. 8. Then validation is also carried
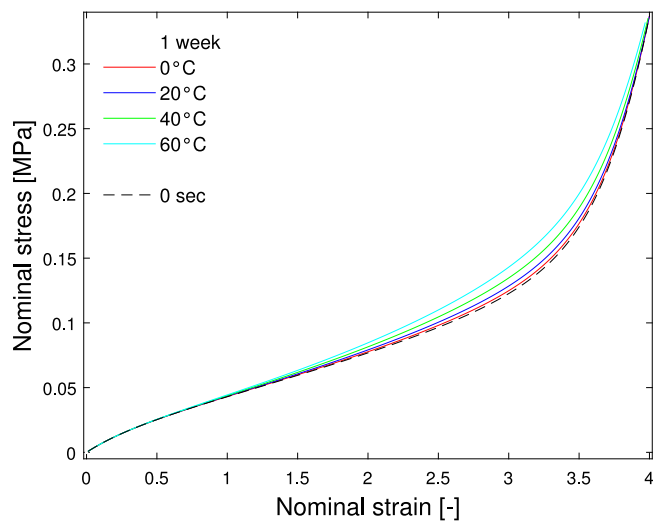
Fig. 9. Modelling validation of the stress–strain curves of re-stretches at different annealing temperatures.
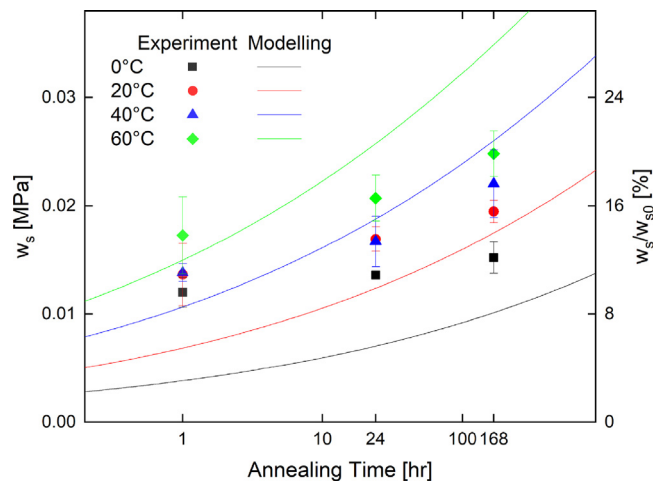

Fig. 10. Comparison of the experimental and modelling results of the dissipation density.

out by predicting the experiments in Fig. 4. The acceleration of stress recovery at higher annealing temperatures is also predicted, as shown in Fig. 9.

Finally, the dissipation can also be simulated, as Fig. 10 shows. The increasing trend at each temperature, the acceleration of stress recovery, and the deviation of the curves at different temperatures are predicted. Our model can simulate the time–temperature equivalent of stress recovery successfully.

5. Conclusions

In this study, we investigate the stress recovery behaviour of the Ecoflex silicone rubber by annealing the specimens at different temperatures with different annealing times after stress softening occurs during the pre-stretch cycle. We find that annealing the specimen after softening at a higher temperature can accelerate the stress recovery process. The stress recovery shows the equivalence of the dependence on annealing time and annealing temperature, conforming to the classical TTS principle. A constitutive model in consideration with a time–temperature-dependent stress recovery is developed based on the model proposed earlier in [37] by adjusting the internal variable η to be dependent on the reduced annealing time. These findings are essential

for the prediction of the stress recovery behaviour of the Ecoflex silicone rubber under different annealing conditions.

Declaration of competing interest

The authors declare that they have no known competing financial interests or personal relationships that could have appeared to influence the work reported in this paper.

Data availability

Data will be made available on request.

References

[1] P. Mazurek, S. Vudayagiri, A.L. Skov, How to tailor flexible silicone elastomers with mechanical integrity: A tutorial review, Chem. Soc. Rev. 48 (6) (2019) 1448–1464, http://dx.doi.org/10.1039/c8cs00963e.

[2] K. Hishikawa, B.S. Oemar, Z. Yang, T.F. Lüscher, Pulsatile stretch stimulates superoxide production and activates nuclear factor-κB in human coronary smooth muscle, Circ. Res. 81 (5) (1997) 797–803, http://dx.doi.org/10.1161/01.RES.81.5.797.

[3] X.Q. Brown, K. Ookawa, J.Y. Wong, Evaluation of polydimethylsiloxane scaffolds with physiologically-relevant elastic moduli: Interplay of substrate mechanics and surface chemistry effects on vascular smooth muscle cell response, Biomaterials 26 (16) (2005) 3123–3129, http://dx.doi.org/10.1016/j.biomaterials.2004.08.009.

[4] R.N. Palchesko, L. Zhang, Y. Sun, A.W. Feinberg, Development of polydimethylsiloxane substrates with tunable elastic modulus to study cell mechanobiology in muscle and nerve, PLoS ONE 7 (12) (2012) e51499, http://dx.doi.org/10.1371/journal.pone.0051499.

[5] A. Unkovskiy, S. Spintzyk, J. Brom, F. Huettig, C. Keutel, Direct 3D printing of silicone facial prostheses: A preliminary experience in digital workflow, J. Prosthet. Dent. 120 (2) (2018) 303–308, http://dx.doi.org/10.1016/j.prosdent.2017.11.007.

[6] G. Soldani, P. Losi, M. Bernabei, S. Burchielli, D. Chiappino, S. Kull, E. Briganti, D. Spiller, Long term performance of small-diameter vascular grafts made of a poly(ether)urethane– polydimethylsiloxane semi-interpenetrating polymeric network, Biomaterials 31 (9) (2010) 2592–2605, http://dx.doi.org/10.1016/j.biomaterials.2009.12.017.

[7] S.C.B. Mannsfeld, B.C.-K. Tee, R.M. Stoltenberg, C.V.H.-H. Chen, S. Barman, B.V.O. Muir, A.N. Sokolov, C. Reese, Z. Bao, Highly sensitive flexible pressure sensors with microstructured rubber dielectric layers, Nature Mater. 9 (10) (2010) 859–864, http://dx.doi.org/10.1038/nmat2834.

[8] L. An, T. Lu, J. Xu, Z. Wang, M. Xu, T.J. Wang, Soft sensor for measuring wind pressure, Int. J. Mech. Sci. 141 (January) (2018) 386–392, http://dx.doi.org/10.1016/j.ijmecsci.2018.01.038.

[9] S. Cheng, B. Chen, Y. Zhou, M. Xu, Z. Suo, Soft sensor for full dentition dynamic bite force, Extreme Mech. Lett. 34 (2020) 100592, http://dx.doi.org/10.1016/j.eml.2019.100592.

[10] M. Amjadi, Y.J. Yoon, I. Park, Ultra-stretchable and skin-mountable strain sensors using carbon nanotubes–Ecoflex nanocomposites, Nanotechnology 26 (37) (2015) 375501, http://dx.doi.org/10.1088/0957-4484/26/37/375501.

[11] S.J. Kim, S. Mondal, B.K. Min, C.-G. Choi, Highly sensitive and flexible strain–pressure sensors with cracked paddy-shaped MoS 2 /graphene foam/Ecoflex hybrid nanostructures, ACS Appl. Mater. Interfaces 10 (42) (2018) 36377–36384, http://dx.doi.org/10.1021/acsami.8b11233.

[12] Y. Jiang, Y. Wang, Y.K. Mishra, R. Adelung, Y. Yang, Stretchable CNTs-Ecoflex composite as variable-transmittance skin for ultrasensitive strain sensing, Adv. Mater. Technol. 3 (12) (2018) 1800248, http://dx.doi.org/10.1002/admt.201800248.

[13] J.-W. Lee, J. Chung, M.-Y. Cho, S. Timilsina, K. Sohn, J.S. Kim, K.-S. Sohn, Deep-learning technique to convert a crude piezoresistive carbon nanotube-ecoflex composite sheet into a smart, portable, disposable, and extremely flexible keypad, ACS Appl. Mater. Interfaces 10 (24) (2018) 20862–20868, http://dx.doi.org/10.1021/acsami.8b04914.

[14] H. Mai, R. Mutlu, C. Tawk, G. Alici, V. Sencadas, Ultra-stretchable MWCNT–Ecoflex piezoresistive sensors for human motion detection applications, Compos. Sci. Technol. 173 (2019) 118–124, http://dx.doi.org/10.1016/j.compscitech.2019.02.001.

[15] M. Cianchetti, C. Laschi, A. Menciassi, P. Dario, Biomedical applications of soft robotics, Nat. Rev. Mater. 3 (6) (2018) 143–153, http://dx.doi.org/10.1038/s41578-018-0022-y.

[16] T.J. Wallin, J. Pikul, R.F. Shepherd, 3D printing of soft robotic systems, Nat. Rev. Mater. 3 (6) (2018) 84–100, http://dx.doi.org/10.1038/s41578-018-0002-2.

[17] S. Krpovic, K. Dam-Johansen, A.L. Skov, Importance of Mullins effect in commercial silicone elastomer formulations for soft robotics, J. Appl. Polym. Sci. 138 (19) (2021) 50380, http://dx.doi.org/10.1002/app.50380.

[18] E. Yarali, M. Baniasadi, A. Zolfagharian, M. Chavoshi, F. Arefi, M. Hossain, A. Bastola, M. Ansari, A. Foyouzat, A. Dabbagh, M. Ebrahimi, M.J. Mirzaali, M. Bodaghi, Magneto-/ electro-responsive polymers toward manufacturing, characterization, and biomedical/ soft robotic applications, Appl. Mater. Today 26 (2022) 101306, http://dx.doi.org/10.1016/j.apmt.2021.101306.

[19] R. Cardoso, A.C. Balestro, A. Dellallibera, E.C.M. Costa, J.M.G. Angelini, L.H.I. Mei, Silicone insulators of power transmission lines with a variable inorganic load concentration: Electrical and physiochemical analyses, Measure.: J. Int. Measure. Confed. 50 (1) (2014) 63–73, http://dx.doi.org/10.1016/j.measurement.2013.12.030.

[20] C.L. Zhang, Z.H. Lai, X.X. Rao, J.W. Zhang, D. Yurchenko, Energy harvesting from a novel contact-type dielectric elastomer generator, Energy Convers. Manage. 205 (2020) 112351, http://dx.doi.org/10.1016/j.enconman.2019.112351.

[21] I. Collins, M. Hossain, W. Dettmer, I. Masters, Flexible membrane structures for wave energy harvesting: A review of the developments, materials and computational modelling approaches, Renew. Sustain. Energy Rev. 151 (2021) 111478, http://dx.doi.org/10.1016/j.rser.2021.111478.

[22] M. Mariello, L. Fachechi, F. Guido, M. De Vittorio, Multifunctional sub-100 Mm thickness flexible piezo/triboelectric hybrid water energy harvester based on biocompatible AlN and soft parylene C-PDMS-Ecoflex™, Nano Energy 83 (2021) 105811, http://dx.doi.org/10.1016/j.nanoen.2021.105811.

[23] L. Mullins, Effect of stretching on the properties of rubber, Rubber Chem. Technol. 21 (2) (1948) 281–300, http://dx.doi.org/10.5254/1.3546914.

[24] J.A.C. Harwood, A.R. Payne, Stress softening in natural rubber vulcanizates. Part III. Carbon black-filled vulcanizates, J. Appl. Polym. Sci. 10 (2) (1966) 315–324, http://dx.doi.org/10.1002/app.1966.070100212.

[25] D.E. Hanson, M. Hawley, R. Houlton, K. Chitanvis, P. Rae, E.B. Orler, D.A. Wrobleski, Stress softening experiments in silica-filled polydimethylsiloxane provide insight into a mechanism for the Mullins effect, Polymer 46 (24) (2005) 10989–10995, http://dx.doi.org/10.1016/j.polymer.2005.09.039.

[26] G. Machado, G. Chagnon, D. Favier, Analysis of the isotropic models of the Mullins effect based on filled silicone rubber experimental results, Mech. Mater. 42 (9) (2010) 841–851, http://dx.doi.org/10.1016/j.mechmat.2010.07.001.

[27] T.-T. Mai, Y. Morishita, K. Urayama, Novel features of the Mullins effect in filled elastomers revealed by stretching measurements in various geometries, Soft Matter 13 (10) (2017) 1966–1977, http://dx.doi.org/10.1039/c6sm02833k.

[28] R.W. Ogden, D.G. Roxburgh, A pseudo– elastic model for the Mullins effect in filled rubber, Proc. R. Soc. Lond. Ser. A Math. Phys. Eng. Sci. 455 (1988) (1999) 2861–2877, http://dx.doi.org/10.1098/rspa.1999.0431.

[29] G. Marckmann, E. Verron, L. Gornet, G. Chagnon, P. Charrier, P. Fort, A theory of network alteration for the Mullins effect, J. Mech. Phys. Solids 50 (9) (2002) 2011–2028, http://dx.doi.org/10.1016/s0022-5096(01)00136-3.

[30] G. Chagnon, On the relevance of continuum damage mechanics as applied to the Mullins effect in elastomers, J. Mech. Phys. Solids 52 (7) (2004) 1627–1650, http://dx.doi.org/10.1016/j.jmps.2003.12.006.

[31] H. Qi, M. Boyce, Stress– strain behavior of thermoplastic polyurethanes, Mech. Mater. 37 (8) (2005) 817–839, http://dx.doi.org/10.1016/j.mechmat.2004.08.001.

[32] G. Machado, G. Chagnon, D. Favier, Induced anisotropy by the Mullins effect in filled silicone rubber, Mech. Mater. 50 (2012) 70–80, http://dx.doi.org/10.1016/j.mechmat.2012.03.006.

[33] R. Dargazany, M. Itskov, Constitutive modeling of the Mullins effect and cyclic stress softening in filled elastomers, Phys. Rev. E 88 (1) (2013) 012602, http://dx.doi.org/10.1103/physreve.88.012602.

[34] R. Raghunath, D. Juhre, M. Klüppel, A physically motivated model for filled elastomers including strain rate and amplitude dependency in finite viscoelasticity, Int. J. Plast. 78 (2016) 223–241, http://dx.doi.org/10.1016/j.ijplas.2015.11.005.

[35] P. Zhu, Z. Zhong, Development of the network alteration theory for the Mullins softening of double-network hydrogels, Mech. Mater. 152 (2021) 103658, http://dx.doi.org/10.1016/j.mechmat.2020.103658.

[36] Z. Liao, M. Hossain, X. Yao, R. Navaratne, G. Chagnon, A comprehensive thermo-viscoelastic experimental investigation of Ecoflex polymer, Polym. Test. 86 (2020) 106478, http://dx.doi.org/10.1016/j.polymertesting.2020.106478.

[37] Z. Liao, M. Hossain, X. Yao, Ecoflex polymer of different Shore hardnesses: Experimental investigations and constitutive modelling, Mech. Mater. 144 (2020) 103366, http://dx.doi.org/10.1016/j.mechmat.2020.103366.

[38] Z. Rigbi, Reinforcement of rubber by carbon black, Rubber Chem. Technol. 55 (4) (1982) 1180–1220, http://dx.doi.org/10.5254/1.3535922.

[39] L. Yan, D.A. Dillard, R.L. West, L.D. Lower, G.V. Gordon, Mullins effect recovery of a nanoparticle-filled polymer, J. Polym. Sci. B 48 (21) (2010) 2207–2214, http://dx.doi.org/10.1002/polb.22102.

[40] S.Y. Zheng, H. Ding, J. Qian, J. Yin, Z.L. Wu, Y. Song, Q. Zheng, Metal-coordination complexes mediated physical hydrogels with high toughness, stick-slip tearing behavior, and good processability, Macromolecules 49 (24) (2016) 9637–9646, http://dx.doi.org/10.1021/acs.macromol.6b02150.

[41] Z. Liao, J. Yang, M. Hossain, G. Chagnon, L. Jing, X. Yao, On the stress recovery behaviour of Ecoflex silicone rubbers, Int. J. Mech. Sci. 206 (2021) 106624, http://dx.doi.org/10.1016/j.ijmecsci.2021.106624.

[42] F. Laraba-Abbes, P. Ienny, R. Piques, A new 'Tailor-made' methodology for the mechanical behaviour analysis of rubber-like materials: II. Application to the hyperelastic behaviour characterization of a carbon-black filled natural rubber vulcanizate, Polymer 44 (3) (2003) 821–840, http://dx.doi.org/10.1016/s0032-3861(02)00719-x.

[43] J. Diani, B. Fayolle, P. Gilormini, A review on the Mullins effect, Eur. Polym. J. 45 (3) (2009) 601–612, http://dx.doi.org/10.1016/j.eurpolymj.2008.11.017.

[44] A. Amin, A. Lion, P. Höfer, Effect of temperature history on the mechanical behaviour of a filler-reinforced NR/BR blend: Literature review and critical experiments, ZAMM - J. Appl. Math. Mech. / Z. Angew. Math. Mech. 90 (5) (2010) 347–369, http://dx.doi.org/10.1002/zamm.200900365.

[45] J. Plagge, M. Klüppel, Mullins effect revisited: Relaxation, recovery and high-strain damage, Mater. Today Commun. 20 (2019) 100588, http://dx.doi.org/10.1016/j.mtcomm.2019.100588.

[46] C. Ma, T. Ji, C.G. Robertson, R. Rajeshbabu, J. Zhu, Y. Dong, Molecular insight into the Mullins effect: Irreversible disentanglement of polymer chains revealed by molecular dynamics simulations, Phys. Chem. Chem. Phys. 19 (29) (2017) 19468–19477, http://dx.doi.org/10.1039/C7CP01142C.

[47] A.M. Stricher, R.G. Rinaldi, C. Barrès, F. Ganachaud, L. Chazeau, How I met your elastomers: From network topology to mechanical behaviours of conventional silicone materials, RSC Adv. 5 (66) (2015) 53713–53725, http://dx.doi.org/10.1039/c5ra06965c.

[48] Z. Li, H. Xu, X. Xia, Y. Song, Q. Zheng, Energy dissipation accompanying Mullins effect of nitrile butadiene rubber/carbon black nanocomposites, Polymer 171 (January) (2019) 106–114, http://dx.doi.org/10.1016/j.polymer.2019.03.043.

[49] C.O. Horgan, R.W. Ogden, G. Saccomandi, A theory of stress softening of elastomers based on finite chain extensibility, Proc. R. Soc. Lond. Ser. A Math. Phys. Eng. Sci. 460 (2046) (2004) 1737–1754, http://dx.doi.org/10.1098/rspa.2003.1248.

[50] D. De Tommasi, G. Puglisi, G. Saccomandi, Micromechanics-based model for the Mullins effect, J. Rheol. 50 (2006) 495, http://dx.doi.org/10.1122/1.2206706.

[51] P. D'Ambrosio, D. De Tommasi, D. Ferri, G. Puglisi, A phenomenological model for healing and hysteresis in rubber-like materials, Internat. J. Engrg. Sci. 46 (4) (2008) 293–305, http://dx.doi.org/10.1016/j.ijengsci.2007.12.002.

[52] D. De Tommasi, S. Marzano, G. Puglisi, G. Zurlo, Damage and healing effects in rubber-like balloons, Int. J. Solids Struct. 46 (22) (2009) 3999–4005, http://dx.doi.org/10.1016/j.ijsolstr.2009.07.020.

[53] D. De Tommasi, G. Puglisi, G. Saccomandi, Damage, self-healing, and hysteresis in spider silks, Biophys. J. 98 (9) (2010) 1941–1948, http://dx.doi.org/10.1016/j.bpj.2010.01.021.

[54] A.F. Blanchard, D. Parkinson, Breakage of carbon-rubber networks by applied stress, Rubber Chem. Technol. 25 (4) (1952) 808–842, http://dx.doi.org/10.5254/1.3543444.

[55] A.D. Drozdov, A. Dorfmann, Finite viscoelasticity of filled rubbers: The effects of pre-loading and thermal recovery, Contin. Mech. Thermodyn. 14 (4) (2002) 337–361, http://dx.doi.org/10.1007/s001610100073.

[56] R. Diaz, J. Diani, P. Gilormini, Physical interpretation of the Mullins softening in a carbon-black filled SBR, Polymer 55 (19) (2014) 4942–4947, http://dx.doi.org/10.1016/j.polymer.2014.08.020.

[57] D. De Tommasi, S. Marzano, G. Puglisi, G. Saccomandi, Localization and stability in damageable amorphous solids, Contin. Mech. Thermodyn. 22 (1) (2010) 47–62, http://dx.doi.org/10.1007/s00161-009-0122-4.

[58] R. Long, K. Mayumi, C. Creton, T. Narita, C.-Y. Hui, Time dependent behavior of a dual cross-link self-healing gel: Theory and experiments, Macromolecules 47 (20) (2014) 7243–7250, http://dx.doi.org/10.1021/ma501290h.

[59] S. Wang, S.A. Chester, Modeling thermal recovery of the Mullins effect, Mech. Mater. 126 (May) (2018) 88–98, http://dx.doi.org/10.1016/j.mechmat.2018.08.002.

[60] L. Mullins, N.R. Tobin, Theoretical model for the elastic behavior of filler-reinforced vulcanized rubbers, Rubber Chem. Technol. 30 (2) (1957) 555–571, http://dx.doi.org/10.5254/1.3542705.

[61] H. Chu, J. Lin, D. Lei, J. Qian, R. Xiao, A network evolution model for recovery of the mullins effect in filled rubbers, Int. J. Appl. Mech. 12 (9) (2020) 2050108, http://dx.doi.org/10.1142/S1758825120501082.

[62] S.R. Lavoie, R. Long, T. Tang, A rate-dependent damage model for elastomers at large strain, Extreme Mech. Lett. 8 (2016) 114–124, http://dx.doi.org/10.1016/j.eml.2016.05.016.

[63] S.C. Lamont, J. Mulderrig, N. Bouklas, F.J. Vernerey, Rate-dependent damage mechanics of polymer networks with reversible bonds, Macromolecules 54 (23) (2021) 10801–10813, http://dx.doi.org/10.1021/acs.macromol.1c01943.

[64] F.J. Vernerey, R. Long, R. Brighenti, A statistically-based continuum theory for polymers with transient networks, J. Mech. Phys. Solids 107 (2017) 1–20, http://dx.doi.org/10.1016/j.jmps.2017.05.016.

[65] L. Zhang, X. Yao, S. Zang, Q. Han, Temperature and strain rate dependent tensile behavior of a transparent polyurethane interlayer, Mate. Des. (1980-2015) 65 (2015) 1181–1188, http://dx.doi.org/10.1016/j.matdes.2014.08.054.

[66] M. Wissler, E. Mazza, Mechanical behavior of an acrylic elastomer used in dielectric elastomer actuators, Sensors Actuators A 134 (2) (2007) 494–504, http://dx.doi.org/10.1016/j.sna.2006.05.024.

[67] M. Hossain, D.K. Vu, P. Steinmann, Experimental study and numerical modelling of VHB 4910 polymer, Comput. Mater. Sci. 59 (none) (2012) 65–74, http://dx.doi.org/10.1016/j.commatsci.2012.02.027.

[68] R. Sahu, K. Patra, J. Szpunar, Experimental study and numerical modelling of creep and stress relaxation of dielectric elastomers, Strain 51 (1) (2014) 43–54, http://dx.doi.org/10.1111/str.12117.

[69] B.D. Coleman, D.C. Newman, On the rheology of cold drawing. I. Elastic materials, J. Polym. Sci. B 26 (9) (1988) 1801–1822, http://dx.doi.org/10.1002/polb.1988.090260901.

[70] B.D. Coleman, D.C. Newman, On the rheology of cold drawing. II. Viscoelastic materials, J. Polym. Sci. B 30 (1) (1992) 25–47, http://dx.doi.org/10.1002/polb.1992.090300104.

[71] D. De Tommasi, G. Puglisi, G. Saccomandi, Localized versus diffuse damage in amorphous materials, Phys. Rev. Lett. 100 (8) (2008) 085502, http://dx.doi.org/10.1103/PhysRevLett.100.085502.

[72] E. Farotti, E. Mancini, A. Lattanzi, M. Utzeri, M. Sasso, Effect of temperature and strain rate on the formation of shear bands in polymers under quasi-static and dynamic compressive loadings: Proposed constitutive model and numerical validation, Polymer 245 (2022) 124690, http://dx.doi.org/10.1016/j.polymer.2022.124690.

[73] W. Tang, D. Li, Y. Peng, P. Wu, Shear band development under simple shear and the intrinsicality of strain softening of amorphous glassy polymers, Polymer 255 (2022) 125115, http://dx.doi.org/10.1016/j.polymer.2022.125115.

[74] Z. Liao, X. Yao, L. Zhang, M. Hossain, J. Wang, S. Zang, Temperature and strain rate dependent large tensile deformation and tensile failure behavior of transparent polyurethane at intermediate strain rates, Int. J. Impact Eng. 129 (2019) 152–167, http://dx.doi.org/10.1016/j.ijimpeng.2019.03.005.

[75] G. Strobl, The Physics of Polymers, third ed., Springer Berlin Heidelberg, Berlin, Heidelberg, 2007, http://dx.doi.org/10.1007/978-3-540-68411-4.

[76] A. Wineman, J.-H. Min, Time dependent scission and cross-linking in an elastomeric cylinder undergoing circular shear and heat conduction, Int. J. Non-Linear Mech. 38 (7) (2003) 969–983, http://dx.doi.org/10.1016/S0020-7462(02)00041-0.

[77] J.D. Ferry, Viscoelastic Properties of Polymers, Wiley, New York, 1980.

[78] R.M. Christensen, Theory of Viscoelasticity: An Introduction, Academic Press, New York, 1971.

[79] M.L. Williams, R.F. Landel, J.D. Ferry, The temperature dependence of relaxation mechanisms in amorphous polymers and other glass-forming liquids, J. Am. Chem. Soc. 77 (14) (1955) 3701–3707, http://dx.doi.org/10.1021/ja01619a008.

[80] K. Kothari, Y. Hu, S. Gupta, A. Elbanna, Mechanical response of two-dimensional polymer networks: Role of topology, rate dependence, and damage accumulation, J. Appl. Mech. 85 (3) (2018) http://dx.doi.org/10.1115/1.4038883.

[81] H. Dal, O. Gultekin, K. Acikoz, An extended eight-chain model for hyperelastic and finite viscoelastic response of rubberlike materials: Theory, experiments and numerical aspects, J. Mech. Phys. Solids 145 (2020) 104159, http://dx.doi.org/10.1016/j.jmps.2020.104159.

[82] H. Dal, B. Canzis, C. Miehe, A three-scale compressible microsphere model for hyperelastic materials, Internat. J. Numer. Methods Engrg. 116 (2018) 412–433, http://dx.doi.org/10.1002/nme.5930.